Biosensors and Bioelectronics 77 (2016) 1086–1094

Contents lists available at ScienceDirect

Biosensors and Bioelectronics

journal homepage: www.elsevier.com/locate/bios

Spin-coated Au-nanohole arrays engineered by nanosphere lithography for a *Staphylococcus aureus* 16S rRNA electrochemical sensor

Agnes Purwidyantri [a], Ching-Hsiang Chen [b], Bing-Joe Hwang [c,d], Ji-Dung Luo [e], Chiuan-Chian Chiou [e], Ya-Chung Tian [f], Chan-Yu Lin [f,g], Chi-Hui Cheng [g,h], Chao-Sung Lai [i,j,*]

[a] *Biomedical Engineering, Chang-Gung University, Taoyuan 333, Taiwan*
[b] *Graduate Institute of Applied Science and Technology, National Taiwan University of Science and Technology, Taipei 106, Taiwan*
[c] *Department of Chemical Engineering, National Taiwan University of Science and Technology, Taipei 106, Taiwan*
[d] *National Synchrotron Radiation Research Center, Hsinchu 300, Taiwan*
[e] *Department of Medical Biotechnology and Laboratory Science, Chang Gung University, Taoyuan 333, Taiwan*
[f] *Kidney Research Center, Department of Nephrology, Chang Gung Memorial Hospital, Taoyuan 333, Taiwan*
[g] *Department of Medicine, Chang Gung University, Taoyuan 333, Taiwan*
[h] *Department of Pediatrics, Division of Pediatric Nephrology, Chang Gung Children's Hospital, Chang Gung Memorial Hospital, Taoyuan 333, Taiwan*
[i] *Department of Electronic Engineering, Chang-Gung University, Taoyuan 333, Taiwan*
[j] *Department of Materials Engineering, Ming-Chi University of Technology, New Taipei City 243, Taiwan*

ARTICLE INFO

Article history:
Received 21 August 2015
Received in revised form
29 October 2015
Accepted 31 October 2015
Available online 2 November 2015

Keywords:
Nanosphere lithography (NSL)
Au-nanohole array
Spin-coated AuNPs
Staphylococcus aureus
16S rRNA
Electrochemical sensor

ABSTRACT

The nanopatterning of gold nanoparticle (AuNP) arrays on an indium tin oxide (ITO) electrode using efficient and low-cost methods is described. This process used nanosphere lithography (NSL) encompassing the deposition of monolayered Polystyrene (PS) followed by a convective self-assembly drop coating protocol onto the ITO substrate that further acted as the mask after the AuNP assembly. The results showed that spin-coating allowed AuNPs to follow the contour and adhere to the PS nanospheres. The final products, after etching the PS, generated a highly ordered Au-nanohole array on an ITO substrate. The Au-nanohole arrays on the ITO electrode provided a greater surface area and successfully enhanced the peak current of electrochemical measurements by 82% compared with bare ITO and was used to detect *Staphylococcus aureus* 16S rRNA hybridization. In contrast to non-templated AuNP structures, the Au-nanohole arrays on the ITO electrode contributed to an optimum sensitivity improvement in DNA hybridization detection by 23%, along with an impressive limit of detection (LOD) of 10 pM. The high specificity of this distinguished structure was also achieved in the hybridization measurements of multi-analyte pathogens. These findings indicate that the combination of PS nanosphere lithography, followed by the spin-coating of AuNPs, leads to an inexpensive and simple engineering process that effectively generates uniform Au-nanohole arrays on ITO, which provides a greater surface area to optimize the electrochemical performance of the DNA biosensor.

1. Introduction

The fabrication of nanoporous electrodes has progressed to feature many vital characteristics, such as a distinctive and controllable structure, a large specific surface area to volume ratio, uniformity, physical rigidity, chemical and thermal stability and high electrical conductivity (Melde and Johnson, 2010; Xu et al., 2012). These excellent properties have led to further investigations of nanoporous metal properties that expand their applications in electrochemical sensing and energy systems (Zhang and Li, 2012), especially in the development of a biosensing platform, such as a DNA sensor. When preparing to construct a DNA sensor, the step involving the immobilization of the DNA probe plays a critical role by contributing to the specificity and sensitivity of the sensor, which also depends primarily on the substrate preparation. Numerous techniques in nanostructuring of the pores, including its downscaling of pore diameter, have greatly attracted research interests. Ahangar and Mehrgardi (2012) observed the application of gold nanoporous electrodes by electrochemical grafting in the detection of DNA mutations. Wang et al. (2011) attempted to identify the morphology of the Au nanoflower by altering the pH

* Corresponding author at: Department of Electronic Engineering, Chang-Gung University, Taoyuan 333, Taiwan.
E-mail address: cslai@mail.cgu.edu.tw (C.-S. Lai).

http://dx.doi.org/10.1016/j.bios.2015.10.094
0956-5663/

of Au precursors for a DNA sensor. Ahn et al. (2013) used an Au film on highly ordered cylindrical AAO (anodic aluminum oxide) with a 30–100-nm diameter via anodization. Daggumati et al. (2015) designed a nanoporous Au thin film using the methods of sputtering, dealloying and high temperature treatment to create a DNA sensing membrane, whereas Hu et al. (2009) developed a nanoporous gold electrode using Au–Ag and an electroless deposition for DNA hybridization detection. Despite the vast number of approaches already used to generate nanoporous electrodes for enhanced DNA sensing performance, the processes for manufacturing nanomaterials and making electrode modifications are relatively complex, resulting in uncontrolled surface morphology and uniformity.

There are two major processes required for the generation of nanoporous electrodes. The first process is the assembly of atoms (from ion reduction) to obtain nanostructures. Then, the masking material is removed from the bulk material, leaving only the desired nanostructures that typically provide a highly defined size, shape and configuration, which is a direct benefit of the templates (Liu et al., 2013; Petryayeva and Krull, 2011). The first process is challenging due to the difficulties in removing large amounts of materials, whereas the second process has complication in generating uniform monolayered particles that support identical points of nanoparticle growth (Petryayeva and Krull, 2011). The use of conventional direct templating, such as the electron beam lithography (EBL) and scanning probe lithography (SPL), can generate arbitrarily shaped particles with various sizes; however, the slow throughput hinders their use in mass production (Ma et al., 2012; Ye et al., 2012). In addition, SPL has limitations in size resolution (approximately 60 nm) and available lasers, and EBL is too expensive for commercial use even though it can produce nanostructures with sizes less than 10 nm without any resolution issues (Haes et al., 2005).

Nanosphere lithography (NSL) is a bottom-up technique in nanoporous material fabrication using a cost-effective synthetic procedure that generates patterns of noble metal nanoparticle arrays in a large area (Ho et al., 2011; Lee et al., 2012; Song and Elsayed-Ali, 2010). Numerous colloidal spheres, such as polystyrene (PS), silica and latex beads, have been serving as templates for porous nanomaterial preparations and have finally produced an arrangement of two-dimensional (2D) and three-dimensional (3D) colloidal crystals (Vakarelski et al., 2009; Li et al., 2012). A monolayer of closely packed PS nanobeads can form in vacant spaces of the template that could be filled with more important materials through several approaches, including physical adsorption, electrodeposition, hydrothermal fabrication and chemical batch deposition (Xia et al., 2012, 2011). This technique is so precise that it can etch various patterns on PS nanobeads. Other remarkable features of the NSL technique include the ease of replication and high monodispersity of the nanostructures assembled for a single or batched sample preparation. The pattern of absorbed nanoparticles on electrodes can vary, for instance: the AuNP structure of nano-triangles and a hollow sphere array is produced through colloidal crystal template-assisted methods (Xiang et al., 2010; Yu et al., 2012) and the triangular nanoparticles array is formed by adding a surfactant and sonicating the sample (Tsigara et al., 2013). These methods are simple, inexpensive and an inherently parallel fabrication of a functionalization process; therefore, NSL has been widely applied in the development of diverse sensors.

In recent decades, metallic nanoparticles, such as gold nanoparticles (AuNPs), with their excellent characteristics regarding adsorption ability, high biocompatibility and great surface area (Rana et al., 2012; Su et al., 2013; Zeng et al., 2011), have been recognized as a prominent candidate in electrochemical sensor development to improve the detection of DNA hybridization, immobilization and intercalation of redox reactions with DNA and increments of electrical conductivity on the surface. In terms of the DNA hybridization investigation, the high load of DNA onto the sensing membrane is not the only factor contributing to highly efficient hybridization. One significant factor is the ability to control the DNA density and scattering onto the sensing surface, which leads to improved electrochemical properties and a beneficial orientation effect (Ben-Yoav et al., 2012). Therefore, enhancing the surface area is a substantial step in the process of DNA detection. Hence, current research is focusing on electrode surface modifications for DNA biosensors that apply the excellence behaviors of AuNPs, for instance Liu et al. (2013) successfully applied template vesicles to further investigate its potency in elevating the DNA load and hybridization efficiency (Liu et al., 2010), and Silvestrini and Ugo, 2013 detected the active surface area of DNA on the nanoelectrode ensembles covered by AuNPs.

NSL patterning methods used to produce AuNP arrays with high periodicity and uniformity in large areas of substrate are promising techniques for building an electrochemical biosensor. Several improvements can be applied to this patterning, including an increased surface area to volume ratio, decreased impedance, sensitivity enhancement, thermal stability, catalytic effects, increased diffusion rates, increased selectivity, lowering of the oxidation potential, signal amplification and faster reaction-response times. Furthermore, metal nanoparticles can play a role in electrochemical reversibility for redox reactions because this process is difficult to produce on the bulk metal electrode (Tsigara et al., 2013). Another protocol for Au deposition besides the NSL includes the deposition of AuNPs onto the PS templated-substrate using spin-coating techniques, but this is rarely reported. Thermally evaporated metal has also been investigated; however, evaporating metal to obtain a very thin film has not been prevalently discussed. Spin-coating has some advantages, for instance, it is rapidly implemented and compatible to wafer-scale processes (Colson et al., 2011). Although the thermal evaporator is considered mainstream, the use of the NSL method for the deposition of a super thin Au film onto a templated-substrate may provide an alternative pathway for growing nanoparticles on patterned surfaces.

Staphylococcus aureus is a commonly isolated pathogen mostly found in patients with indwelling medical devices, such as in patients receiving peritoneal dialysis (PD). The bacterial infection induces severe peritonitis (Johnson et al., 2014; Najafi et al., 2013; Wolley et al., 2012) and contributes to approximately 18% of infection-related mortality in PD patients (Li et al., 2010). Furthermore, studies have revealed the presence of a short bacteria-derived DNA in the dialysis fluid (Ahmadi et al., 2013; Shin et al., 2011; Szeto et al., 2015) and this DNA contains the non-methylated CpG motif that triggers inflammation through the monocyte and lymphocyte Toll-like receptor 9 (Glorieux et al., 2012; Schiffl, 2011; Szeto et al., 2013). Among bacterial DNA fragments, the 16S rRNA gene sequence exhibits robust properties for highly accurate identification of bacterial isolates and the discovery of novel bacteria in clinical microbiology laboratories. In regards to bacterial identification, the 16S rRNA is necessary to detect bacteria with unusual phenotypic profiles, rare bacteria, slowly growing bacteria, uncultivable bacteria and culture-negative infections (Ahmadi et al., 2013; Michael and Abbott, 2007; Szeto et al., 2013, 2015; Woo et al., 2008). Conventional bacterial identification methods, such as polymerase chain reaction (PCR), culture and colony counting, immunological techniques and fluorescence-based assays, are disadvantageous because they are laborious, complex and time-consuming processes. Therefore, developing a DNA sensor that is rapid, miniaturized, sensitive and has accurate detection of 16S rRNA sequences with specific probes, may emerge as a promising breakthrough.

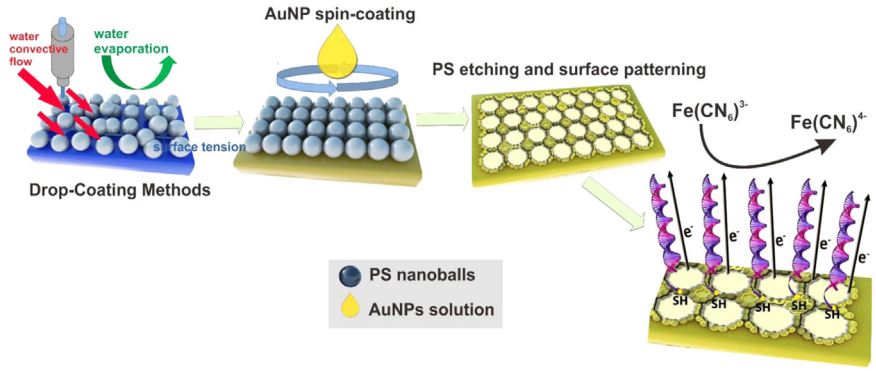

Fig. 1. Schematic illustration of the strategy for engineering the highly ordered Au-nanohole arrays on ITO on a glass substrate using PS nanospheres as a mask and its application for the electrochemical DNA sensor.

Herein, we engineered Au-nanohole arrays using two different techniques: by randomly scattering AuNPs on ITO and by spin-coating a AuNP solution to generate the NSL patterned-ITO substrate. The electrodes were tested for electrochemical detection in *S. aureus* 16S rRNA using a unique set of probes from *S. aureus* 16S rRNA designed by our team. We created the AuNP array with inherent shapes and tunable sizes independent of the PS sphere's size using both AuNP deposition methods, and this yielded specific replicable topological features corresponding to the surface area responsible for electrochemical responses in DNA detection using CV measurements, a commonly used measurement method that obtains information about the redox potential and electrochemical reaction rates (e.g., the chemical rate constant) of analyte solutions (Grieshaber et al., 2008).

The results demonstrated that the proposed electrochemical sensor, generated by spin-coating AuNPs, amplified the electrochemical signal more effectively than the non-patterned one. This approach also had an excellent specificity against the non-complementary bacterial target DNA and high reproducibility. The surface topology and morphology were both distinguished through different AuNP deposition methods. The detection of DNA hybridization signals is tested with the AuNP array prepared by different methods. Finally, we designed this simple, cost effective, high-throughput nanofabrication production of highly ordered Au-nanohole arrays on an ITO electrode, which enhanced the electrochemical performance of the DNA sensor.

2. Materials and methods

2.1. Materials

The ITO on a glass substrate (thickness of 0.7 mm and a sheet resistance of 7 Ω/square) was purchased from Uni-Onward (Taipei, Taiwan). The micro particle size standard based on polystyrene monodisperse (diameter = 500 nm) and phosphate buffered saline (PBS) were purchased from Sigma Aldrich (St. Louis, MO, USA). Dodecyl sodium sulfate and potassium chloride were purchased from Merck (Darmstadt, Germany). Potassium ferricyanide was purchased from Nihon Shiyaku Industries Ltd. (Taipei, Taiwan). Acetone, iso propyl alcohol (IPA) and toluene were purchased from Avantor (Pennsylvania, USA). The gold nanoparticle solution with a diameter of 13 nm was prepared by NTUST (Taipei, Taiwan). The synthetic thiolated oligonucleotide probe of *S. aureus* 16S rRNA and its complementary sequence and the *Escherichia coli* and *Pseudomonas aeruginosa* 16S rRNA complementary sequences were ordered from Purigo Biotech Inc. (Taipei, Taiwan). The experimental solutions were prepared with deionized 18.2 MΩ cm water provided by a MilliQ system.

2.2. Apparatus

The spin-coater used to deposit AuNPs was a Swienco type PM -90. The ultrasonic cleaner used for substrate cleaning was CREST 950 D (Crest Ultrasonic Corp, New Jersey, USA). The oxygen plasma cleaner was from Harrick Plasma (New York, USA). The images were taken with a field emission-scanning electron microscope (FE-SEM) HITACHI S-4700 (Japan). Cyclic Voltammetry (CV) was conducted using a 611E Electrochemical Analyzer from CH Instruments, Inc. (Austin, TX, USA).

2.3. Assembly of the Au-nanohole array on an ITO electrode

For the entire experimental process, the ITO on a glass substrate was cut into pieces of 1×1 cm^2, sonicated in DI H_2O, washed with acetone and IPA sequentially and dried with a N_2 flow. Prior to adding the PS monolayer covering, the ITO on a glass substrate was treated with O_2 plasma to make it more hydrophilic. Pattern grafting on a substrate was schematically depicted in Fig. 1. First, a 2% wt. solution of PS nanospheres was prepared, and 10 μL of the solution was drop cast onto the surface of the ITO immersed in ultrapure water. Next, approximately 5 μL of 2% Dodecyl sodium sulfate solution was added to alter the surface tension of the water; thus, the monolayer of PS nanospheres were pushed aside toward the targeted ITO substrate. As a result, the monolayer of PS nanospheres attached to approximately 90% of the ITO substrate during a gentle and careful substrate tilting (45° angle) with a tweezer. The substrate was then sequentially dried at room temperature, in an 80 °C incubator and on a 100 °C hot plate for 30 min, 30 min and 2 min, respectively, to reduce the clustering of PS nanospheres.

The monolayer PS nanospheres were then used as a mask for the AuNP growth pattern. A 100 μL of the 15 nM AuNP solution with AuNP diameters of 13 nm was spin-coated for 30 s with 2000 rpm velocity. Subsequently, the substrate incubated overnight in a dark room to maintain the AuNP stability on the ITO substrate. The PS nanobeads were further etched away by the immersion of the substrates in toluene; therefore, the final structure of a highly ordered honeycomb-like hexagonal AuNP array was engineered. These substrates were subsequently used in the electrochemical detection of DNA hybridization.

2.4. Electrochemical detection of S. aureus 16S rRNA hybridization

A single strand of a thiolated oligonucleotide probe (ssHS-probe; for targeting *S. aureus* 16S rRNA) with a concentration of 1 μM in 1 × PBS (PBS: 10 mM phosphate buffer, 137 mM NaCl, 2.7 mM KCl, pH 7.4) was immobilized on the modified ITO electrode for 16 h at room temperature. Complementary target DNA

was added and incubated for 1 h at 37 °C to hybridize with the probe. DNA hybridization was carried out in 1% PBS. To check the specificity and sensitivity of the sensor, the mixture containing 100 nM of the complementary sequence from *S. aureus* and 1 μM of the non-specific sequences from *E. coli* or *P. aeruginosa* were measured. The stability and reproducibility of the substrate were tested with a CV curve for the hybridization of the *S. aureus* probe DNA with its complementary target DNA at 1 nM using three different substrates. The electrochemical measurement was conducted with a conventional three-electrode system consisting of Ag/AgCl (saturated with KCl) as a reference, the Au-nanohole arrays-ITO electrode was working and the platinum wire was a counter electrode using the CHI 611E potentiostat. To confirm the surface modification of the sensor, cyclic voltammograms were recorded between 0 and 0.4 V at a scan rate of 50 mV/s for 50 cycles in a solution containing 5 mM $K_3[Fe(CN)_6]/K_4[Fe(CN)_6]$ and 0.5 M KCl for each step of elemental deposition.

2.5. Designing the DNA sequence

The 16S rRNA sequences of all *S. aureus, E. coli,* and *P. aeruginosa* were obtained from the Ribosomal Database Project II database. The consensus 16S rRNA sequence for each bacterium resulted multiple alignments and randomly cleaved into 40-nucleotide fragments. The fragments were then aligned with sequences of all three bacteria. Only fragments matching $>90\%$ of their original bacteria and $<10\%$ of other bacteria were used for the following experiments (Table 1).

3. Results and discussion

This study successfully recorded the step-by-step morphology alterations of ITO substrates using the NSL strategy as is shown in the manipulation pathway sketched in Fig. 1. The ITO was found to be very attractive and extensively utilized in the construction of optoelectronic platforms, touch panels, solar cells, transparent electrodes for liquid crystal displays and electrochemical sensors (Jung et al., 2008; Lue et al., 2012; Rashid et al., 2014; Stanculescu and Stanculescu, 2007). Due to these common uses, the ITO substrate was preferably employed as the foundation to grow AuNPs with the convective self-assembly drop-coating PS NSL protocol.

We observed a relatively large area of the substrate was well covered by the PS balls after using the drop-coating method, which also showed uniformity and great order. Among various techniques, including drop-coating convective self-assembly, dip-coating, spin-coating, controlled meniscus and bar-coating, the drop-coating convective self-assembly is known to show versatility in the form of closely packed arrays dominated by capillary immersion forces where it is able to infiltrate sol–gel or other solution phase precursors into the template particle arrays, in such conditions where the spin-coating method is difficult to generate. Instead, spin-coating method, for evaporation induced array formation starting at the substrate border, forms crystals with different principal orientations merging, creating domain boundaries and a monolayer of particles is not easily produced (Giuliani et al., 2010; Jeong et al., 2010). The consistent uniformity and high-order of the template has indicated that the PS NSL is more efficient and less expensive for depositing highly uniform particles compared with other deposition pathways completed in our previous work using RF sputtering to directly deposit hafnium oxide (HfO_2) on silicon structure of EIS (Lai et al., 2006).

In Fig. 2(A) and (B), high uniformity of PS nanobeads deposited onto the bare ITO were obtained, shown by the color contrast from various orientations of the sphere arrays. From our previous studies, we know that the common methods to introduce target materials to the PS templates include physical and chemical vapor phase syntheses, such as evaporation and sputtering, physical and chemical vapor deposition (PVD, CVD) and atomic layer deposition (ALD). Conversely, spin-coating AuNPs onto a roughened surface has not been well-explored. In this paper, Fig. 2(C) clearly displays that the spin-coated AuNPs have a tendency to follow the topography of the PS balls and adhere to them instead of filling the interstices within the single PS nanobead. The bright center depicts the PS and the darker edge was the AuNP molecules. Once PS beads were etched away, the honey-comb like Au-nanohole array was formed highly ordered as seen in Fig. 2(D). The hexagonal array of Au-nanoholes successfully covered a relatively large area of the substrate with sufficient distribution, despite the existence of some defected points. The structure imperfections could be a consequence of the absorption intensity limitation due to the formation of only monolayers of nanoparticles (Eustis and El-Sayed, 2006). The TEM figure of AuNPs with a diameter of 13 nm used in this study is presented in Fig. 2(E). Moreover, the energy dispersive X-ray spectroscopy (EDX) analysis in Fig. 2(F) also confirmed the nanopore element was Au on ITO. The Au-nanohole arrays via electroless plating on metal seed-anchored colloidal crystals were successfully formed by the Au aggregation process. The aggregated metal structure had a greater surface area than the solid spheres, conferred a nanometer edge and entropically resisted the assembly into close packed structures, thus, a super hydrophobic substrate was produced (Liu et al., 2013). The spin-coated Au created a nanohole diameter of approximately 385 nm, which is considerably small compared with other studies listed in Table 2. To be used in electrochemical measurements, the smaller pores contribute to greater sensitivity and performance (Kant et al., 2014).

Both the non-patterned and patterned Au-nanohole arrays were subsequently used as electrochemical DNA sensors. The electrochemical behavior of the electroactive $Fe(CN)_6^{3-/4-}$ redox couple was used to reflect the electron transfer characteristics of the electrode for the *S. aureus* 16S rRNA hybridization test. We choose CV as our analytical electrochemistry parameter because it is known as the most versatile electrochemical method for many redox active metal complexes, which are not amenable to various spectroscopic methods, either because of weak absorption bands (forbidden d–d transitions) or because of the overlap of electronic transitions with those of the DNA molecules (Arjmand et al., 2011).

The 16S rRNA gene sequence is recognized as a critical marker for infections in patients with implanted medical devices, like in PD patients where extracellular DNA fragments prevalently appear (Ahmadi et al., 2013; Schiffl, 2011; Szeto et al., 2015). A novel sequential design of the distinctive 16S rRNA from several bacteria has isolated sequences from *S. aureus, E. coli* and *P. aeruginosa*, as was screened in this research. This gene represents the most prevalent housekeeping genetic marker and is large enough for

Table 1
Synthetic oligonucleotides representing the designed 16S rRNA gene sequence of *S. Aureus, E. coli* and *P. aeruginosa.*

	S. aureus	*E. coli*	*P. aeruginosa*
Probe	5′HS-AAA AAA GTT ATC CCA GTC TTA TAG GTA GGT 3′ (30 mer)	5′HS-AAA AAG TCC ACG CCG TAA ACG ATG TCG ACT TGG 3′ (33 mer)	5′HS-AAA AAC AGC CAT GCC GCG TGT GTG AAG AAG GTC 3′ (33 mer)
Target	5′ACC TAC CTA TAA GAC TGG GAT AAC T 3′ (25 mer)	5′CCA AGT CGA CAT CGT TTA CGG CGT GGA C 3′ (28 mer)	5′ GAC CTT CTT CAC ACA CGC GGC ATG GCT G 3′ (28 er)
Random Target	5′CGC CGT AAA CGA TGT CGA CT 3′ (20 mer)		

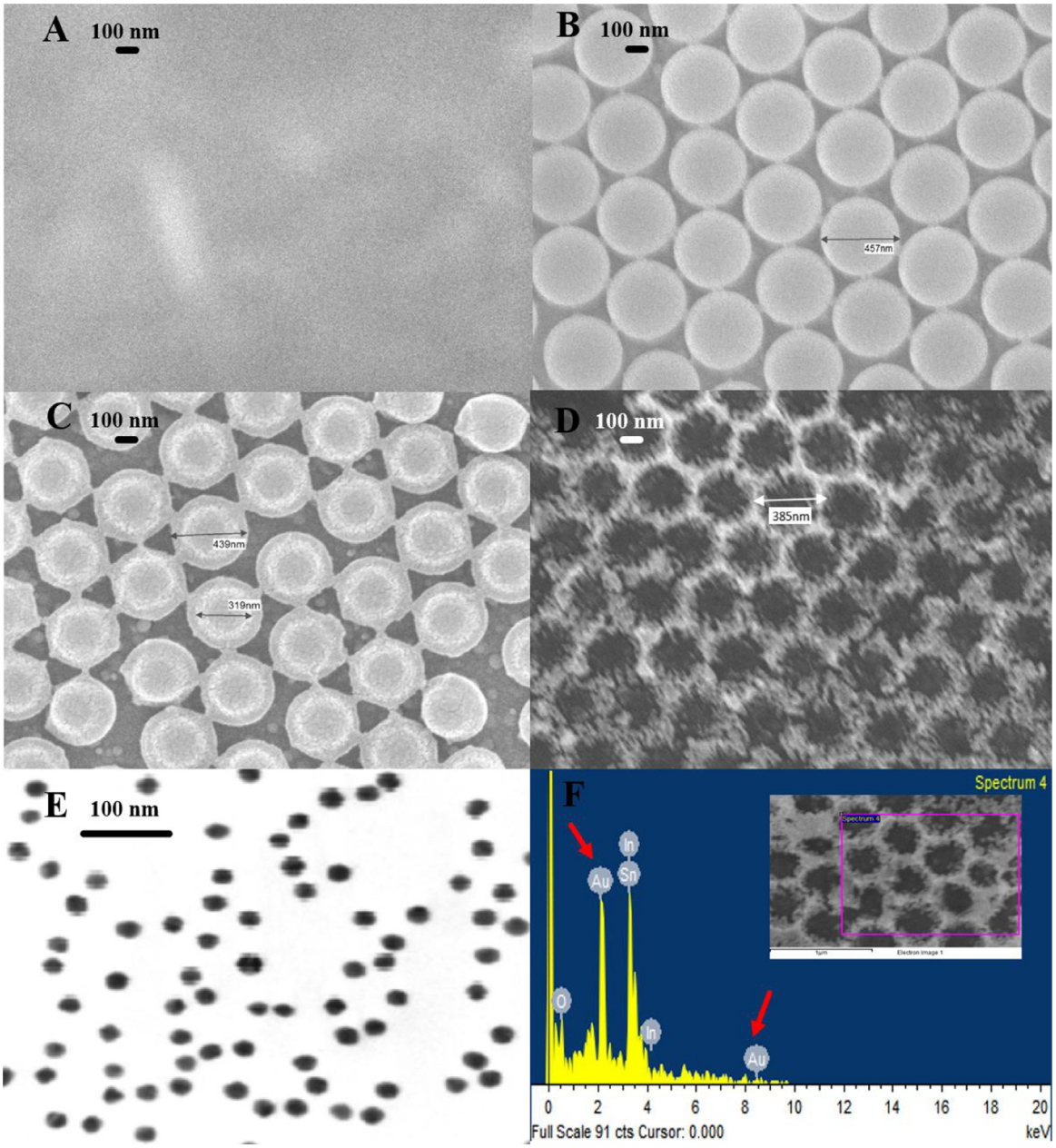

Fig. 2. SEM images of the morphological features for the step-by-step engineering of Au-nanohole arrays on the ITO electrode: (A) bare ITO, (B) uniform distribution of PS nanospheres deposited onto the ITO substrate, (C) spin-coated AuNP growth on the PS-covered ITO substrate, (D) Au-nanohole arrays on the ITO substrate after PS etching with toluene, (E) TEM image of AuNPs with a diameter of 13 nm used in all experimental settings, and (F) EDX spectrum validation of the Au element deposited onto the ITO substrate.

informatics purposes (1500 bp) (Janda and Abbott, 2007; Li et al., 2010; Szeto et al., 2013). The comparison was done between the ITO electrode with a random configuration of AuNPs and one with the Au-nanohole arrays. Fig. 3(A) and (B) depicted the cyclic voltammogram acquired from the ITO electrode with randomly scattered AuNPs and Au-nanohole arrays on its surface. The peak current value (ΔI_p) after the deposition of the honeycomb-like AuNP structure was significantly enhanced by approximately 82% compared with the bare ITO (Fig. 3(B)). On the contrary, in Fig. 3 (A), the deposition of non-templated AuNPs on an ITO substrate showed an increase of only approximately 14% from its bare ITO state. This remarkable outcome reveals the fact that nanoporous materials exhibit higher surface area. In addition, it has been cited by (Xia et al., 2011) that the nanoporous configuration was able to reach several square meters for a thin film of only one centimeter across. Due to the enhanced surface area, many porous electrodes were shown to greatly increase the sensitivity of the electrochemical signal (Ahangar and Mehrgardi, 2012; Daggumati et al., 2015; Melde and Johnson, 2010; Xu et al., 2012). Furthermore, the shift of peak potential difference (ΔE_p) after DNA hybridization in both structures was resulted in the cyclic voltammograms. As for the honeycomb-like AuNP array on an ITO, a pair of redox peaks consisting of $Fe(CN)_6^{3-/4-}$ emerged at 0.314 V and 0.187 V giving a formal potential $E^{0'}$ of 0.250 V and the peak potential difference (ΔE_p) of 0.127 V. After the immersion of 1 μM ss-DNA, a decrease in the redox peak current and an increase in the ΔE_p were visible, attributed from the modification of the AuNP array with the 5′-end of thiolated DNA (via gold-thiol bond) blocking the interfacial electron transfer between the gold surface and bulk solution (Kashefi-Kheyrabadi and Mehrgardi, 2013; McEwen et al., 2009;

Table 2
Feature comparisons between the proposed Au-nanohole arrays on an ITO electrode and other reported nanopore-based techniques for the electrochemical detection of DNA hybridization.

Au pore diameter (nm)	Uniformity/ Monodispersity	AuNP deposition methods	Concentration of AuNPs used	Duration of AuNP deposition	Analytical technique	Range of detection (nM)	Fabrication Cost	References
600	Monolayer	Electroplating	5.10^6 nM	> 3–4 min	Cyclic voltammetry	1000	Medium	Li et al. (2012)
n.a.	Non-uniform	Thermal evaporation	250 nm thickness	> 60 min	Square wave voltammetry	10–100	High	Daggumati et al. (2015)
60–130	Multilayer	Anodization	gold CDtrode	> 5 min	Differential pulse voltammetry	2500	High	Ahangar and Mehrgardi (2012)
20	Non-uniform	Selective dissolution	Au/Ag alloy, 50:50 wt%, 100 nm thick	> 1 h	Differential pulse voltammetry	0.0009–0.07	High	Hu et al. (2009)
385	Highly uniform and monolayer	Convective self-assembly NSL and spin-coating of AuNPs	15 nM	30 s	Cyclic voltammetry	0.01–1000	Low	This method

Wang et al., 2011).

The sensitivity validation of the Au-nanohole arrays as a DNA biosensor was accomplished by linearity test normalization of the peak current value (ΔI_p) per AuNP surface area, calculated with this following equation:

$$\Delta I_p(\text{Normalization}) = \frac{\Delta I_p \text{ samples}}{\Delta I_p \text{ AuNP deposited ITO} - \Delta I_p \text{ bare ITO}}$$

The normalization was done with the consideration that the major impact in the alteration of the peak current solely resulted from the deposited AuNPs. Thus, the comparison addressed the condition of the ITO substrate with deposited AuNPs and the bare ITO substrate. As plotted in Fig. 3(C) and (D), the coefficient correlations of the electrochemical peak current value resulted from both randomly scattered AuNPs and Au-nanohole arrays on an ITO electrode for *S. aureus* 16S rRNA hybridization showed significant linearity ($R > 0.95$) (Illanes, 2008). Fig. 3(C) displays the normalized peak current obtained by the non-templated AuNP modifications onto the ITO electrode, which showed lower sensitivity when compared with the Au-nanohole arrays (Fig. 3(D)), even though the AuNPs seemed to respond to the elevating concentration of target DNA hybridization linearly. The AuNP modifications offered higher surface area of sensing, however, the crowdedness of the particles affected the hybridization efficiency because it is correlated to the space provided for the DNA landing point and orientation. Fig. 3(D) illustrates that the honeycomb-like AuNP array had significantly improved the sensitivity of the DNA hybridization in the electrochemical sensing system by approximately 23%, shown by the 1.365 arb. unit/nM target. Furthermore, the honeycomb-like AuNP array electrode also consequently reached the limit of detection (LOD), which was 10 pM for the DNA target and defined an obvious improvement from the LOD generated by the random configuration of AuNPs (46 pM). The sensitivity and smaller LOD obtained by the Au-nanohole structure may be pertinent for clinical samples because the detectable values are far below that of a typically measured infected peritoneal concentration of cell-free DNA in severe peritonitis, ranging from 2 to 10 mg/L (Pajek et al., 2010). In patients receiving peritoneal dialysis, the detection of very small DNA concentrations of circulating pathogens is urgently required to give a prognosis of early bacterial infection (Li et al., 2010; Szeto et al., 2013, 2007, 2015).

The existence of specific configurations of the AuNPs provides a higher surface area to volume ratio and significantly enhances the load of the DNA probe onto the sensor surface with its precise molecular orientation (Ben-Yoav et al., 2012; Liu et al., 2010). From the electrochemical improvement, the Au-nanohole array supplies more effective surface density of the DNA probes onto the interface compared with the disoriented AuNPs. In low probe density regions, 100% of hybridization is possibly reached, and comparatively faster binding kinetics are present. In contrast, at the high-density probe regions, the hybridization efficiency is much lower, and the kinetics are slower. Nevertheless, the hybridization isotherms complexity persists and is unable to be fixed with simple kinetics models (Henry and O'Sullivan, 2012; Peterson et al., 2001). Therefore, the assembly of a particular shape of nanoparticles, such as the Au-nanohole arrays performed in this research, may be a versatile and effective method to tailor and control the surface probe density and increase its accessibility to hybridize complementary targets. Moreover, the proposed honeycomb-like Au-nanohole arrays in this study were also compared with other DNA electrochemical biosensors employing Au nanoporous structure as listed in Table 2. The proposed sensor showed more uniform and highly ordered structures engineered with quicker processes altogether that were simpler and less expensive (only using 15 nM of AuNP solution for 100 μL per electrode) yet continued to reach a

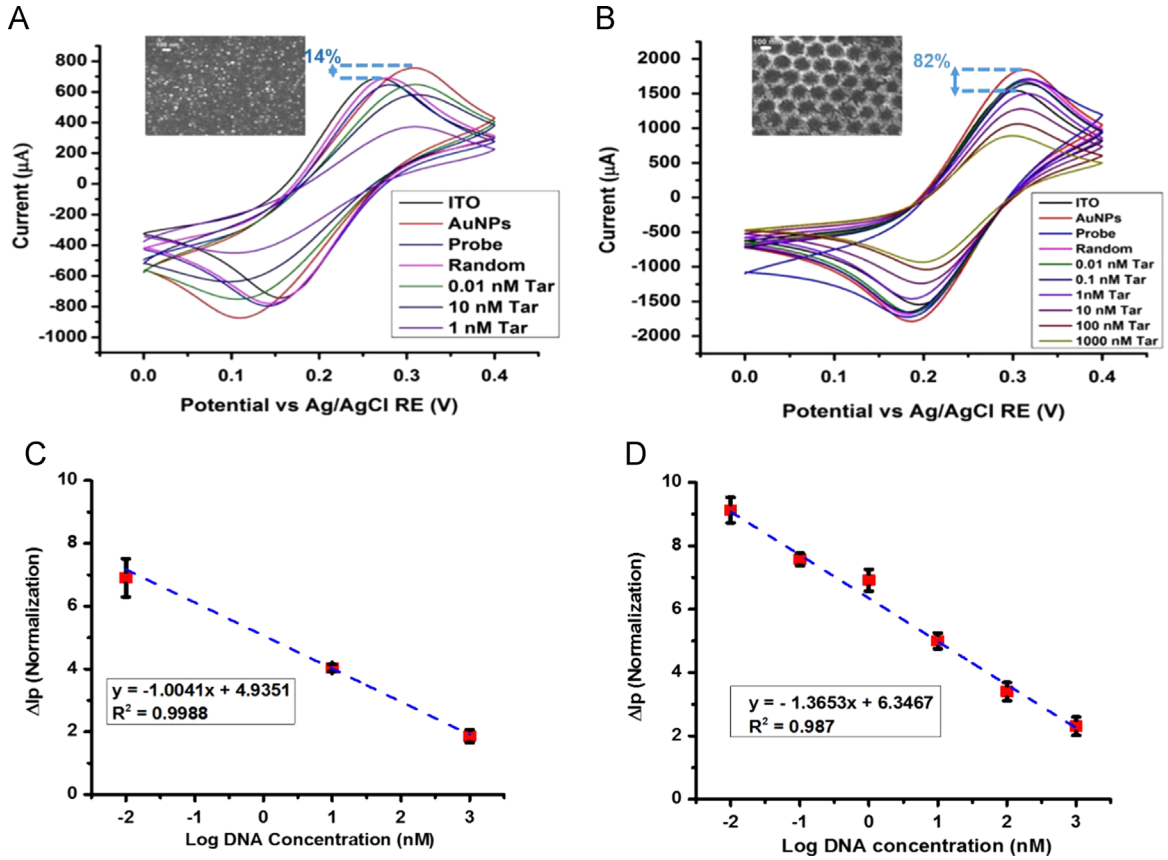

Fig. 3. The Cyclic Voltammogram (CV) between 0 and 0.4 V at a scan rate of 50 mV/s in 5 mM $K_3[Fe(CN)_6]/K_4[Fe(CN)_6]$ and 0.5 M KCl. of *S. aureus* 16S rRNA hybridization using (A) randomly-scattered AuNPs on an ITO electrode, Inset: SEM image of randomly scattered AuNPs on an ITO electrode, (B) Au-nanohole arrays on an ITO electrode, Inset: SEM image of the honeycomb-like AuNP array on an ITO electrode, with normalized sensitivity and linearity of the peak current (ΔI_p) for *S. aureus* 16S rRNA hybridization detection using (C) randomly scattered AuNPs on an ITO electrode and (D) Au-nanohole arrays on an ITO electrode.

comparable electrochemical DNA sensing range.

In *Staphylococcal* detection, the protocol is not only the issue but also the platform specificity towards specific pathogens. Based on this concept, one of the most pivotal aspects to take into account for the analytical application of the biosensor is the study of the effects from potential interfering agents. The response variation of the *S. aureus* detection on the Au-nanohole arrays on an ITO sensor was conducted by comparing the signals obtained from the complementary target of 100 nM of *S. aureus* 16S rRNA and a mixture of this target with 1000 nM of *E. coli* and *P. aeruginosa*, which are the other prevalent pathogens found in patients with implanted medical instruments. As displayed in Fig. 4(A), it shows that even with the presence of either the 16S rRNA sequence of *E. coli* or *P. aeruginosa* with a 10-fold higher concentration than the complementary target of *S. aureus* 16S rRNA, the signal remained stable compared with that previously obtained in the absence of those two interfering pathogens and with negligible signal changes among the three conditions. These results imply that the immobilized ss-DNA probe selectively bound to the complementary *S. aureus* 16S rRNA target with a minimum chance of disruption from the other emerging sequences of other pathogens that typically exist in real clinical samples. This suggests that the proposed

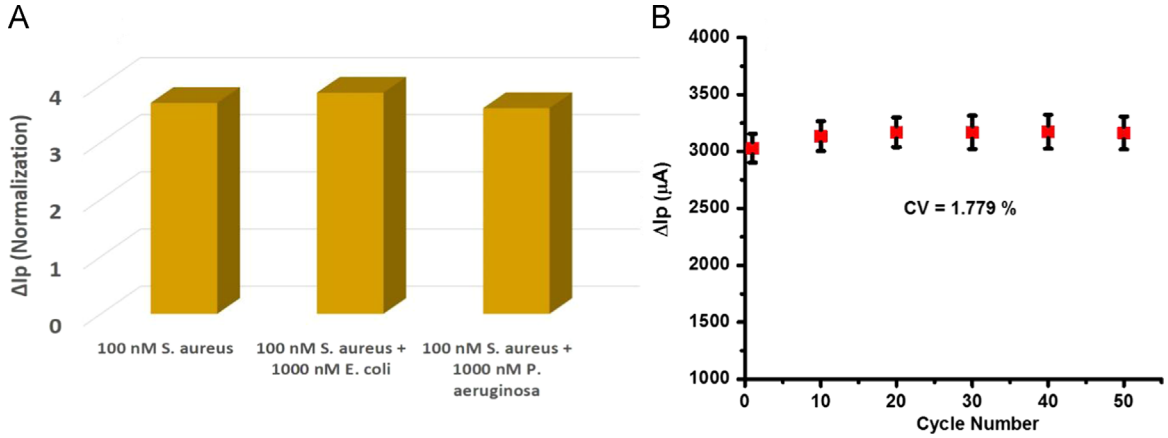

Fig. 4. (A) Specificity performance of Au-nanohole arrays on an ITO electrode for *S. aureus* 16S rRNA hybridization with interferences from *E. coli* and *P. aeruginosa* 16S rRNA sequences and (B) the stability of the peak current (ΔI_p) of *S. aureus* 16S rRNA hybridization with a 1 nM target from 3 substrates at different cycle points, both parameters were run between 0 and 0.4 V at a scan rate of 50 mV/s in 5 mM $K_3[Fe(CN)_6]/K_4[Fe(CN)_6]$ and 0.5 M KCl using Au-nanohole arrays on an ITO electrode.

honeycomb-like AuNP array on an ITO electrochemical DNA sensor could be used as a simultaneous multianalyte-sensing platform.

To confirm the stability and reproducibility, CV measurements were conducted to detect hybridization of complementary *S. aureus* 16S rRNA with a 1 nM target using the proposed Au-nanohole arrays on an ITO (Supplementary material Fig. S1). Fig. 4 (B) demonstrates a stable ΔI_p with a significant coefficient of variation (CV) (less than 2%) resulting from three different substrates at various numbers of cycles, ranging from 3000 to 3200 μA. This reflects that the sensor possesses excellent stability and reproducibility even for such a high cycling set up and with low nucleotide concentrations.

4. Conclusion

An electrochemical sensing enhancement on the detection of *S. aureus* 16S rRNA was successfully developed using the construction of Au-nanohole arrays on an ITO electrode. The integration of convective self-assembly drop-coating PS NSL as the backbone of the Au-nanohole arrays created patterning with simple and brief spin-coating of the AuNP solution, as was demonstrated with the ease of replication and high monodispersity leading to high-throughput products allowing the production of low-cost disposable units. Moreover, the specificity against non-complementary sequences from other pathogens with higher concentration, including *E. coli* and *P. aeruginosa*, was performed. Overall, these results provide insight for the use of this sensor in assisting physicians who deal with clinical samples and need to prescribe the most suitable antibiotics for the patients based on the pathogen(s) involved in the infection. The proposed structure can be regarded as a potential candidate in the development of other sensing platforms, such as field effect transistor (FET)-based or optical-based biosensing devices.

Acknowledgments

The authors thank the Chang Gung Memorial Hospital for the financial support under contract no. of CMRPD2D0072 and CMRPD3D0112.

Appendix A. Supplementary material

Supplementary data associated with this article can be found in the online version at http://dx.doi.org/10.1016/j.bios.2015.10.094.

References

Ahangar, L.E., Mehrgardi, M.A., 2012. Nanoporous gold electrode as a platform for the construction of an electrochemical DNA hybridization biosensor. Biosens. Bioelectron. 38, 252–257.
Ahmadi, S.H., Neela, V., Hamat, R.A., Goh, B.L., Syafinaz, A.N., 2013. Rapid detection and identification of pathogens in patients with continuous ambulatory peritoneal dialysis (CAPD) associated peritonitis by 16s rRNA gene sequencing. Trop. Biomed. 30, 602–607.
Ahn, J., Cho, S., Min, J., 2013. Impedance spectroscopy of highly ordered nanoporous electrodes based on Au-AAO (anodic aluminum oxide) structure. J. Nanosci. Nanotechnol. 13, 7482–7486.
Arjmand, F., Aziz, M., Tabassum, S., 2011. Cyclic voltammetry-an electrochemical approach to study metal-based potential antitumor drug-DNA interaction. Curr. Anal. Chem. 7, 71–79.
Ben-Yoav, H., Dykstra, P.H., Bentley, W.E., Ghodssi, R., 2012. A microfluidic-based electrochemical biochip for label-free diffusion-restricted DNA hybridization analysis. Biosens. Bioelectron. 38, 114–120.
Colson, P., Cloots, R., Henrist, C., 2011. Experimental design applied to spin coating of 2D colloidal crystal masks: a relevant method? Langmuir 27, 12800–12806.
Daggumati, P., Matharu, Z., Seker, E., 2015. Effect of nanoporous gold thin film morphology on electrochemical DNA sensing. Anal. Chem. 87, 8149–8156.
Eustis, S., El-Sayed, M.A., 2006. Why gold nanoparticles are more precious than pretty gold: noble metal surface plasmon resonance and its enhancement of the radiative and nonradiative properties of nanocrystals of different shapes. Chem. Soc. Rev. 35, 209–217.
Giuliani, M., Gonzalez-Vinas, W., Poduska, K.M., Yethiraj, A., 2010. Dynamics of crystal structure formation in spin-coated colloidal films. J. Phys. Chem. Lett. 1, 1481–1486.
Glorieux, G., Neirynck, N., Veys, N., Vanholder, R., 2012. Dialysis water and fluid purity: more than endotoxin. Nephrol. Dial. Transpl. 11, 4010–4021.
Grieshaber, D., MacKenzie, R., Vörös, J., Reimhult, E., 2008. Electrochemical biosensors-sensor principles and architectures. Sensors 8, 1400–1458.
Haes, A.J., Zhao, J., Zou, S., Own, C.S., Marks, L.D., Schatz, G.C., Van Duyne, R.P., 2005. Solution-phase, triangular Ag nanotriangles fabricated by nanosphere lithography. J. Phys. Chem. B 109, 11158–11162.
Henry, O.Y.F., O'Sullivan, C.K., 2012. Rapid DNA hybridization in microfluidics. TrAC Trends Anal. Chem. 33, 9–22.
Ho, Y.H., Chen, K.Y., Liu, S.W., Chang, Y.T., Huang, D.W., Wei, P.K., 2011. Transparent and conductive metallic electrodes fabricated by using nanosphere lithography. Org. Electron. Phys. Mater. Appl. 12, 961–965.
Hu, K., Liu, P., Ye, S., Zhang, S., 2009. Ultrasensitive electrochemical detection of DNA based on PbS nanoparticle tags and nanoporous gold electrode. Biosens. Bioelectron. 24, 3113–3119.
Illanes, A., 2008. Enzyme Biocatalysis: Principles and Applications, Enzyme Biocatalysis: Principles and Applications. Springer, Netherlands.
Janda, J.M., Abbott, S.L., 2007. 16S rRNA gene sequencing for bacterial identification in the diagnostic laboratory: pluses, perils, and pitfalls. J. Clin. Microbiol. 45, 2761–2764. http://dx.doi.org/10.1128/JCM.01228-07.
Jeong, G.H., Park, J.K., Lee, K.K., Jang, J.H., Lee, C.H., Kang, H.B., Yang, C.W., Suh, S.J., 2010. Fabrication of low-cost mold and nanoimprint lithography using polystyrene nanosphere. Microelectron. Eng. 87, 51–55.
Johnson, D.W., Badve, S.V., Pascoe, E.M., Beller, E., Cass, A., Clark, C., de Zoysa, J., Isbel, N.M., McTaggart, S., Morrish, A.T., Playford, E.G., Scaria, A., Snelling, P., Vergara, L.A., Hawley, C.M., 2014. Antibacterial honey for the prevention of peritoneal-dialysis-related infections (HONEYPOT): a randomised trial. Lancet Infect. Dis. 14, 23–30.
Jung, W.S., Yoon, S.G., Kang, S.M., Kim, S.W., Yoon, D.H., 2008. Electrical and optical properties of ITO:Ca composite thin films for TEOLED cathode. Thin Solid Films 516, 5445–5448.
Kant, K., Pries, C., Shapter, J.G., Dusan, L., 2014. The influence of nanopore dimensions on the electrochemical properties of nanopore arrays studied by impedance spectroscopy. Sensors 14, 21316–21328.
Kashefi-Kheyrabadi, L., Mehrgardi, M.A., 2013. Aptamer-based electrochemical biosensor for detection of adenosine triphosphate using a nanoporous gold platform. Bioelectrochemistry 94, 47–52.
Lai, C.-S., Yang, C.-M., Lu, T.-F., 2006. Thickness effects on pH response of HfO_2 sensing dielectric improved by rapid thermal annealing. Jpn. J. Appl. Phys. 45, 3807–3810.
Lee, Y.-R., Alam, M.M., Jung, W.-G., 2012. Fabrication of nano patterns on various substrates using nanosphere lithography technique. J. Nanosci. Nanotechnol. 12, 1211–1215.
Li, P.K.-T., Szeto, C.C., Piraino, B., Bernardini, J., Figueiredo, A.E., Gupta, A., Johnson, D. W., Kuijper, E.J., Lye, W.-C., Salzer, W., Schaefer, F., Struijk, D.G., 2010. Peritoneal dialysis-related infections recommendations: 2010 update. J. Int. Soc. Perit. Dial. 30, 393–423.
Liu, S., Liu, J., Han, X., Cui, Y., Wang, W., 2010. Electrochemical DNA biosensor fabrication with hollow gold nanospheres modified electrode and its enhancement in DNA immobilization and hybridization. Biosens. Bioelectron. 25, 1640–1645.
Liu, Y., Goebl, J., Yin, Y., 2013. Templated synthesis of nanostructured materials. Chem. Soc. Rev. 42, 2610–2653.
Lue, C.E., Wang, I.S., Huang, C.H., Shiao, Y.T., Wang, H.C., Yang, C.M., Hsu, S.H., Chang, C.Y., Wang, W., Lai, C.S., 2012. PH sensing reliability of flexible ITO/PET electrodes on EGFETs prepared by a roll-to-roll process. Microelectron. Reliab. 52, 1651–1654.
Ma, R., Lu, N., Liu, L., Wang, Y., Shi, S., Chi, L., 2012. Fabrication of single gold particle arrays with pattern directed electrochemical deposition. ACS Appl. Mater. Interfaces 4, 3779–3783.
McEwen, G.D., Chen, F., Zhou, A., 2009. Immobilization, hybridization, and oxidation of synthetic DNA on gold surface: electron transfer investigated by electrochemistry and scanning tunneling microscopy. Anal. Chim. Acta 643, 26–37.
Melde, B.J., Johnson, B.J., 2010. Mesoporous materials in sensing: morphology and functionality at the meso-interface. Anal. Bioanal. Chem. 398, 1565–1573.
Michael, Janda, Abbott, Sharon L., 2007. MINIREVIEW: 16S rRNA gene sequencing for bacterial identification in the diagnostic laboratory: pluses, perils, and pitfalls. J. Clin. Microbiol. 45, 2761–2764.
Najafi, I., Alatab, S., Atabak, S., Nouri Majelan, N., Sanadgol, H., Makhdoomi, K., Ardalan, M.R., Azmandian, J., Shojaee, A., Keshvari, A., Hosseini, M., 2014. Seventeen years' experience of peritoneal dialysis in Iran: first official report of the Iranian peritoneal dialysis registry. Perit. Dial. Int. 34, 636–642.
Pajek, J., Kveder, R., Guček, A., Škoberne, A., Bren, A., Bučar, M., Černe, D., Lukač-Bajalo, J., 2010. Cell-free DNA in the peritoneal effluent of peritoneal dialysis solutions. Ther. Apher. Dial. 14, 20–26.
Peterson, A.W., Heaton, R.J., Georgiadis, R.M., 2001. The effect of surface probe density on DNA hybridization. Nucleic Acids Res. 29, 5163–5168.
Petryayeva, E., Krull, U.J., 2011. Localized surface plasmon resonance: nanostructures, bioassays and biosensing—a review. Anal. Chim. Acta 706, 8–24.

Rana, S., Bajaj, A., Mout, R., Rotello, V.M., 2012. Monolayer coated gold nanoparticles for delivery applications. Adv. Drug Deliv. Rev. 64, 200–216.
Rashid, J.I.A., Azah, Y.N., Jaafar, A., Hashim, U., Hajiana, R., 2014. The utilization of SiNWs/AuNPs-modified indium tin oxide (ITO) in fabrication of electrochemical DNA sensor. Mater. Sci. Eng. C 45, 270–276.
Schiffl, H., 2011. High-flux dialyzers, backfiltration, and dialysis fluid quality. Semin. Dial. 24, 1–4.
Shin, J.H., Kim, S.H., Jeong, H.S., Oh, S.H., Kim, H.R., Lee, J.N., Yoon, Y.C., Kim, Y.W., Kim, Y.H., 2011. Identification of coagulase-negative staphylococci isolated from continuous ambulatory peritoneal dialysis fluid using 16S ribosomal RNA, tuf, and SodA gene sequencing. Perit. Dial. Int. 31, 340–346. http://dx.doi.org/10.3747/pdi.2010.00073.
Silvestrini, M., Ugo, P., 2013. Ensembles of nanoelectrodes modified with gold nanoparticles: characterization and application to DNA-hybridization detection. Anal. Bioanal. Chem. 405, 995–1005.
Song, Y., Elsayed-Ali, H.E., 2010. Aqueous phase Ag nanoparticles with controlled shapes fabricated by a modified nanosphere lithography and their optical properties. Appl. Surf. Sci. 256, 5961–5967.
Stanculescu, A., Stanculescu, F., 2007. Investigation of the properties of indium tin oxide-organic contacts for optoelectronic applications. Thin Solid Films 515, 8733–8737.
Su, W., Kim, S.-E., Cho, M., Nam, J.-D., Choe, W.-S., Lee, Y., 2013. Selective detection of endotoxin using an impedance aptasensor with electrochemically deposited gold nanoparticles. Innate Immun. 19, 388–397.
Szeto, C.C., Chow, K.M., Kwan, B.C.H., Law, M.C., Chung, K.Y., Yu, S., Leung, C.B., Li, P.K.T., 2007. Staphylococcus aureus peritonitis complicates peritoneal dialysis: review of 245 consecutive cases. Clin. J. Am. Soc. Nephrol. 2, 245–251.
Szeto, C.-C., Kwan, B.C.-H., Chow, K.-M., Lai, K.-B., Kwok, J.S.-S., Cheng, P.M.-S., Pang, W.-F., Ng, J.K.-C., Chan, M.H.-M., Lit, L.C.-W., Leung, C.-B., Li, P.K.-T., 2015. Circulating bacterial-derived DNA fragment level is a strong predictor of cardiovascular disease in peritoneal dialysis patients. PloS One 10, e0125162.
Szeto, C.C., Lai, K.B., Ching-Ha, B.K., Chow, K.M., Leung, C.B., Law, M.C., Yu, V., Li, P.K.T., 2013. Bacteria-derived DNA fragment in peritoneal dialysis effluent as a predictor of relapsing peritonitis. Clin. J. Am. Soc. Nephrol. 8, 1935–1941.
Tsigara, A., Benkhial, A., Warren, S., Akkari, F., Wright, J., Frehill, F., Dempsey, E., 2013. Metal microelectrode nanostructuring using nanosphere lithography and photolithography with optimization of the fabrication process. Thin Solid Films 537, 269–274.
Vakarelski, I.U., Chan, D.Y.C., Nonoguchi, T., Shinto, H., Higashitani, K., 2009. Assembly of gold nanoparticles into microwire networks induced by drying liquid bridges. Phys. Rev. Lett. 102, 058303.
Wang, L., Chen, X., Wang, X., Han, X., Liu, S., Zhao, C., 2011. Electrochemical synthesis of gold nanostructure modified electrode and its development in electrochemical DNA biosensor. Biosens. Bioelectron. 30, 151–157. http://dx.doi.org/10.1016/j.bios.2011.09.003.
Wolley, M.J., Taylor, S.L., Hossain, F., Abbas, S.A., Marshall, M.R., 2012. Association between antimicrobial locks for hemodialysis central venous catheters and antibiotic resistance. Hemodial. Int. 16 (Suppl 1), S2–S9.
Woo, P.C.Y., Lau, S.K.P., Teng, J.L.L., Tse, H., Yuen, K.-Y., 2008. Then and now: use of 16S rDNA gene sequencing for bacterial identification and discovery of novel bacteria in clinical microbiology laboratories. Clin. Microbiol. Infect.: Off. Publ. Eur. Soc. Clin. Microbiol. Infect. Dis. 14, 908–934.
Xia, X., Luo, J., Zeng, Z., Guan, C., Zhang, Y., Tu, J., Zhang, H., Fan, H.J., 2012. Integrated photoelectrochemical energy storage: solar hydrogen generation and supercapacitor. Sci. Rep. 2, 981.
Xia, X., Tu, J., Mai, Y., Wang, X., Gu, C., Zhao, X., 2011. Self-supported hydrothermal synthesized hollow Co_3O_4 nanowire arrays with high supercapacitor capacitance. J. Mater. Chem. 21, 9319–9325.
Xiang, G., Zhang, N., Zhou, X., 2010. Localized surface plasmon resonance biosensing with large area of gold nanoholes fabricated by nanosphere lithography. Nanoscale Res. Lett. 5, 818–822.
Xu, Q., Yin, L., Hou, C., Liu, X., Hu, X., 2012. Facile fabrication of nanoporous platinum by alloying-dealloying process and its application in glucose sensing. Sens. Actuators B Chem. 173, 716–723.
Li, Yanhua, Zeng, Dongming, Chen, Qiyuan, Zhang, Shiying, Yu, Qumin, Xu, D., 2012. Fabrication of honeycomb gold arrays for enhancement of electrochemical performance. Int. J. Electrochem. Sci. 7, 12207–12217.
Ye, J., Wen, F., Sobhani, H., Lassiter, J.B., Dorpe, P., Van, Nordlander, P., Halas, N.J., 2012. Plasmonic nanoclusters: near field properties of the Fano resonance interrogated with SERS. Nano Lett. 12, 1660–1667.
Yu, J., Geng, C., Zheng, L., Ma, Z., Tan, T., Wang, X., Yan, Q., Shen, D., 2012. Preparation of high-quality colloidal mask for nanosphere lithography by a combination of air/water interface self-assembly and solvent vapor annealing. Langmuir 28, 12681–12689.
Zeng, S., Yong, K.-T., Roy, I., Dinh, X.-Q., Yu, X., Luan, F., 2011. A review on functionalized gold nanoparticles for biosensing applications. Plasmonics 6, 491–506.
Zhang, J., Li, C.M., 2012. Nanoporous metals: fabrication strategies and advanced electrochemical applications in catalysis, sensing and energy systems. Chem. Soc. Rev. 41, 7016–7031.